Human Molecular Genetics, 2005, Vol. 14, No. 20 ***3065–3078***
doi:10.1093/hmg/ddi340
Advance Access published on September 23, 2005

Contribution of nuclear and extranuclear polyQ to neurological phenotypes in mouse models of Huntington's disease

Caroline L. Benn[1,5], Christian Landles[1], He Li[2], Andrew D. Strand[3], Ben Woodman[1], Kirupa Sathasivam[1], Shi-Hua Li[2], Shabnam Ghazi-Noori[1], Emma Hockly[1], Syed M.N.N. Faruque[4], Jang-Ho J. Cha[5], Paul T. Sharpe[4], James M. Olson[3], Xiao-Jiang Li[2] and Gillian P. Bates[1,*]

[1]King's College London, Medical and Molecular Genetics, GKT School of Medicine, London SE1 9RT, UK, [2]Department of Genetics, Emory University, Atlanta, GA 30322, USA, [3]Fred Hutchinson Cancer Research Center, University of Washington, Seattle, WA 98109, USA, [4]King's College London, Craniofacial Development, Dental School, London SE1 9RT, UK and [5]MassGeneral Institute for Neurodegenerative Disease, Massachusetts General Hospital, Harvard Medical School, Boston, MA 02139, USA

Received July 15, 2005; Revised and Accepted September 7, 2005

In postmortem Huntington's disease brains, mutant htt is present in both nuclear and cytoplasmic compartments. To dissect the impact of nuclear and extranuclear mutant htt on the initiation and progression of disease, we generated a series of transgenic mouse lines in which nuclear localization or nuclear export signal sequences have been placed N-terminal to the htt exon 1 protein carrying 144 glutamines. Our data indicate that the exon 1 mutant protein is present in the nucleus as part of an oligomeric or aggregation complex. Increasing the concentration of the mutant transprotein in the nucleus is sufficient for and dramatically accelerates the onset and progression of behavioral phenotypes. Furthermore, nuclear exon 1 mutant protein is sufficient to induce cytoplasmic neurodegeneration and transcriptional dysregulation. However, our data suggest that cytoplasmic mutant exon 1 htt, if present, contributes to disease progression.

INTRODUCTION

Huntington's disease (HD) is an autosomal dominant, neurodegenerative disorder with symptom onset usually in mid-life, comprising movement, cognitive and psychiatric impairments inexorably progressing to death within two decades (1). The HD mutation is a CAG repeat expansion in exon 1 of the *HD* gene, which translates into a polyglutamine (polyQ) tract in the huntingtin (htt) protein. HD neuropathology is characterized by generalized brain atrophy, selective neuronal cell death predominantly in the striatum and intracellular polyQ aggregates (2–4). HD is one of an increasing number of inherited neurodegenerative disorders caused by polyQ expansion, which includes spinal and bulbar muscular atrophy (SBMA), dentatorubral pallidoluysian atrophy (DRPLA) and the spinocerebellar ataxias (SCA) types 1, 2, 3, 6, 7 and 17 (5).

In HD patients, polyQ aggregation is present mainly in the form of dystrophic neurites and neuropil aggregates (2,4). Although the frequency of nuclear inclusions increases in juvenile cases, extranuclear aggregation still predominates (2). The R6/2 transgenic mouse line expresses exon 1 htt with expanded polyQ repeats and displays a progressive neurological phenotype that recapitulates a remarkable number of features of the human disorder (6–8). They exhibit an early onset and rapid progression of the phenotype, partly because the CAG repeat size is one that would cause childhood onset in humans, but also because the expression of an N-terminal fragment has most likely by-passed the processing of huntingtin, thought to be an early event in the molecular pathology of the disease (9). The R6/2 mouse has been studied extensively and has recently led to the identification of hypothalamic changes (10) and a muscle pathology

*To whom correspondence should be addressed at: King's College London, Medical and Molecular Genetics, GKT School of Medicine, 8th Floor Guy's Tower, Guy's Hospital, London SE1 9RT, UK. Tel: +44 2071883722; Fax: +44 2071882585; Email: gillian.bates@genetics.kcl.ac.uk

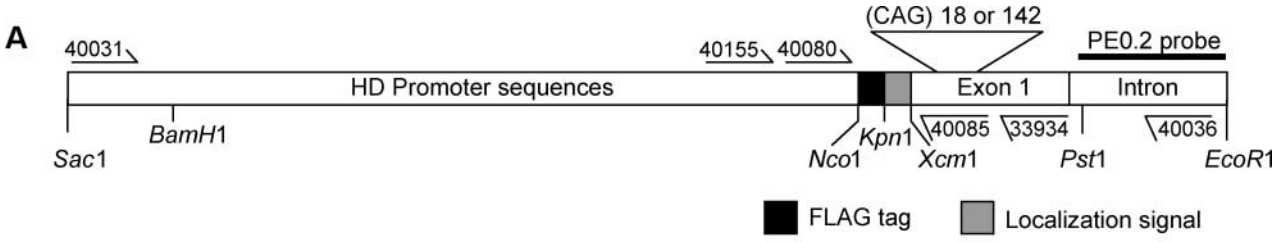

B

Signal	Amino acid sequence
Wild type NLS signal	PPK**K**KRKVDV
Mutant NLS signal	PPK<u>T</u>KRKVDV
Wild type NES signal	A**L**QKK**L**EE**L**E**L**D
Mutant NES signal	A<u>A</u>QKK<u>A</u>EE<u>A</u>E<u>A</u>D

Figure 1. Constructs used for generation of transgenic mouse lines (**A**) A FLAG tag (DYKKDDDK) and localization signal were added to constructs previously used to generate the R6 and HDex transgenic lines. Primer positions used for genotyping or sequencing, the PE0.2 hybridization probe and major restriction enzyme sites are indicated. (**B**) NLS, mutant NLS (mutNLS), NES and mutant NES (mutNES) amino acid sequences are listed. Bold type represents amino acids critical to wild-type function, whereas underlined amino acids are those that have been mutated to abolish the wild-type function.

(11) in HD patients. Nuclear inclusions and neuropil aggregates are present in R6/2 mouse brains prior to symptom onset (12,13), with extranuclear aggregate accumulation correlating more closely with phenotype progression than with nuclear inclusion formation (13). Although it is not known which form of the expanded, misfolded, oligomeric or aggregated protein represents the most toxic polyQ species, the detection of visible aggregates within a subcellular compartment is indicative of the presence of the various forms of the mutant protein.

Experimental data have suggested that the toxicity exerted by expanded polyQ is influenced by its subcellular localization (14), and the consequence of targeting mutant versions of expanded polyQ to the nucleus in different protein contexts has been investigated *in vivo*. Ataxin 1 is a nuclear protein and forms nuclear aggregates in a SCA1 transgenic mouse model and SCA1 patient brains. Transgenic mice expressing an ataxin 1 construct, in which the nuclear localization signal (NLS) had been destroyed, did not develop a neurological phenotype (15). Translocation of the mutant androgen receptor to the nucleus, following the binding of hormone, is essential for disease pathogenesis in a mouse model of SBMA (16). In addition, the appearance of nuclear inclusions and onset of behavioral abnormalities was goaded by increasing levels of HprtQ150 protein in the nucleus, whereas decreasing nuclear levels led to a delay in both of these phenotypes (17). These reports suggest that targeting polyQ expansions to the nucleus accelerates disease onset and progression. In contrast, it was recently reported that directing the N-terminal 171 amino acids of htt with 82Q to the nucleus delayed phenotype onset (18).

The impact of nuclear and extranuclear mutant htt on the initiation and progression of disease remains unclear. We have generated transgenic mouse lines in which NLS or nuclear export signal (NES) sequences have been placed N-terminal to the htt exon 1 protein (transprotein) carrying 144Q. This generated two sets of lines, one in which the mutant transprotein was restricted to the nucleus (NLS144) and the other in which it was present in both the nucleus and the cytoplasm (NES144). The mutant transprotein was only present in the nucleus as part of an aggregation complex. We found that targeting the mutant transprotein to the nucleus dramatically accelerated the onset and progression of behavioral phenotypes for any comparable RNA expression level. Obvious cytoplasmic neurodegeneration in the form of degenerate organelles and dystrophic neurites was present in both sets of lines and can therefore be caused by mutant htt in the nucleus. Comparison of well-matched NLS144 and NES144 lines for the onset and progression of behavioral phenotypes, cytoplasmic degeneration and microarray gene expression profiles indicated that extranuclear mutant htt also contributes to disease pathogenesis.

RESULTS

Generation of transgenic mouse lines

To dissect the contribution of a nuclear or extranuclear localization of expanded polyQ, we generated constructs that fused previously well-characterized NLS or NES with the exon 1 htt protein (Fig. 1A). Like the R6 lines, the transgene was under the control of human HD promoter sequences (6). Localization signals were placed at the N-terminus of the exon 1 protein downstream of a FLAG tag. The sequence encoding the NLS was from the SV40 large T-antigen (19) and that encoding the NES was from MAPKK (20,21), and control constructs contained mutated localization signals (Fig. 1B). Each construct was prepared with 142 and 18 CAG repeats and named according to the localization signal and the polyQ repeat size in the transprotein as follows: NLS144, mutNLS144, NES144, mutNES144, NLS20 and NES20.

The number of founders arising from the microinjection of these constructs, CAG repeat sizes and the subsequently established lines are summarized in Table 1. All potential

Table 1. Summary of transgenic lines

Construct	Founders	Established lines	Lines expressing transgene	Lines analyzed	Founder CAG rpts.
NLS144	6	5	4	Line 25	143
				Line 46	142
				Line 52	142
mutNLS144	6	3	3	Line 16	142
NLS20	4	3	3	Line 50	18
NES144	8	7	6	Line 39	143
				Line 61	142
				Line 68	142
mutNES144	4	4	3	Line 14	143
NES20	2	0	N/A	N/A	18

founders were mated; however, one of each of the NLS144, NES144 and NLS20 founders, three of the mutNLS144 and both of the NES20 founders failed to transmit the transgene to the F1 generation. Therefore, we did not succeed in establishing any lines carrying the NES20 construct. RT–PCR was performed to assay transgene expression, and lines with the highest expression levels were selected for further analysis as follows: NLS144: lines 25, 46 and 52; NES144: lines 39, 61 and 68; NLS20: line 50. The expression level was slightly higher in mutNLS144 line 16 than in mutNES144 line 14. As each of these lines would be expected to function equally well as a control to detect phenotype modifications arising purely through the addition of the FLAG tag and localization sequences (compared with the R6 lines), mutNLS144 line 16 was chosen for use as the control in the detailed analyses that follow.

Comparative transgene expression analyses

Transgenic mice express exon 1 human htt in addition to the endogenous murine wild-type htt. To quantify the transgene mRNA levels, we performed real-time RT–PCR [real-time quantitative PCR (RQ-PCR)]. The highest level of expression occurred in NES144 line 39 (Fig. 2A), with NLS144 line 25, mutNLS144 line 16 and NLS20 line 50 also showing high levels. mRNA levels are normalized to R6/2 expression levels for comparison. These results concurred with those obtained by Phosphoimager quantification of northern blots hybridized with the transgene-specific PE0.2 probe and standardized against GAPDH (data not shown).

RNA was prepared from various brain regions (brainstem, cerebellum, cerebral cortex, hippocampus, olfactory bulb, striatum, thalamus) and peripheral tissues (heart, kidney, liver, lung, skeletal muscle, spleen, gonads), and RT–PCR confirmed that the transgene was ubiquitously expressed in all cases (data not shown). Furthermore, *in situ* hybridization for transgenic mRNA (Fig. 2B) revealed no gross differences in the pattern of expression within the brain for all of the lines (Fig. 2B and C).

NLS results in the accumulation of aggregated protein in the nucleus

To assess subcellular localization signal effects at the protein level, nuclear and cytoplasmic fractions were prepared from whole brain homogenates and used for western blotting (Fig. 2D–G). Blots were routinely reprobed with antibodies to proteins with uniquely nuclear or cytoplasmic distributions to confirm that the fractions were cleanly separated. There is an inherent difficulty of ensuring that high molecular weight cytoplasmic aggregates do not sediment with the nuclear fraction. We therefore complemented the western analysis by chronicling the regional and subcellular distribution of polyQ aggregate neuropathology by immunohistochemistry (Fig. 3) focusing on striatum, cerebral cortex, hippocampus and cerebellum. Brain sections were immunostained with EM48 and S830 (which detect exon 1 htt), ubiquitin and FLAG antibodies.

A specific band corresponding to soluble exon 1 protein was never detected in either nuclear or cytoplasmic fractions prepared from NLS144 lines 25, 46 or 52 irrespective of age or disease state (Fig. 2D). Inspection of the stacking gel suggested that aggregated transprotein had been retained in nuclear but not in cytoplasmic fractions (Fig. 2E). The amount of aggregation seen in the stacking gel does not correlate with the amount of protein in the nucleus, rather it represents protein accumulation over time. Immunohistochemistry confirmed that the NLS had restricted the mutant transprotein to the nucleus (Fig. 3A, D, G and J), where the nuclear pathology first appeared as a granular nuclear stain which progressed to one that included small puncta and finally to a pronounced nuclear inclusion. As soluble bands in the nuclear fraction were never detected for the NLS144 lines, it would appear that all these forms of the nuclear transprotein represent an aggregated state. Relative transgene expression levels (by RQ-PCR) in the NLS144 lines correlated with the order in which the nuclear pathology appeared, e.g. polyQ coalescence occurred earlier and progressed faster in line 25 than in line 46.

Analysis of the NLS20 line 50 revealed soluble transprotein in the cytoplasmic fraction only (Fig. 2G, upper arrow). This can be compared with the smaller cytoplasmic protein seen in Hdex6 and Hdex27 lines expressing exon 1 htt protein with 20Q, without additional FLAG tag or localization sequences (Fig. 2G, lower arrow) (6,12). There was no aggregated transprotein in the stacking gels in either nuclear or cytoplasmic fractions at any time point (up to 16 months). Similarly, immunohistochemistry on NLS20 line 50 brains did not reveal an aggregate pathology with any antibodies at any time point up to 15 months (Fig. 3F and L).

NES failed to exclude the mutant transprotein from the nucleus

A soluble protein was observed only in cytoplasmic fractions from the NES144 lines 39, 61 (Fig. 2D) and 68 (data not shown) at all ages throughout the disease process. Unfortunately, this did not indicate that the NES sequence had successfully exported all of the transprotein from the nucleus as aggregated protein was retained in the stacking gel of both nuclear and cytoplasmic fractions for all NES144 lines (data not shown) (Fig. 2F). An identical pattern of immunoreactivity was seen for mutNLS144 line 16 (data not shown) (Fig. 2D). Immunohistochemistry confirmed the presence of both nuclear and extranuclear polyQ pathologies (Fig. 3B, C, E, H, I and K). The same range and

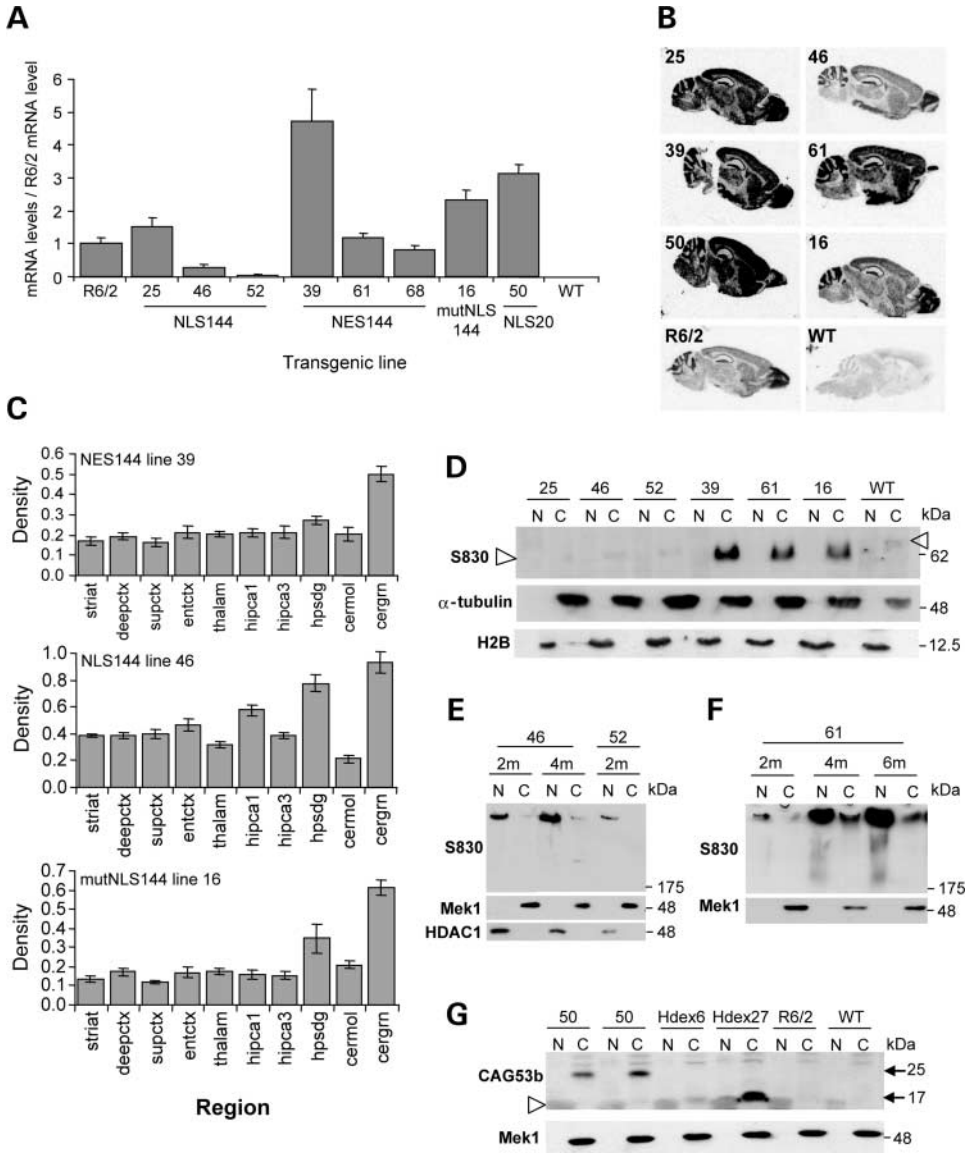

Figure 2. Expression analysis of transgenic mouse lines. (**A**) mRNA prepared from the cerebral cortex of mice at 2 months of age was used for RQ-PCR. The mean number of transgene and of β-actin mRNA molecules were calculated for each line and transgene levels normalized to β-actin. mRNA levels for all lines are shown as a ratio of R6/2. NES144: line 39 ($n = 7$), line 61 ($n = 7$), line 68 ($n = 6$); NLS144: line 25 ($n = 5$), line 46 ($n = 6$), line 52 ($n = 5$); NLS20 line 50 ($n = 7$); mutNLS144 line 16 ($n = 5$) and R6/2 ($n = 6$). Error bars are standard error of the mean (SEM). (**B**) mRNA *in situ* hybridization with a transgene-specific probe was performed on two intact sections from each of six normal and six transgenic mouse brains from each line to analyze the regional expression level. Sections were exposed for several consecutive time periods of different length, and representative non-saturated images were selected which best demonstrated the expression patterns. Shown are NLS144 lines 25 and 46 (top panels), NES144 lines 39 and 61 (second row), NLS20 line 50, mutNLS144 line 16 (third row), R6/2 and a wild-type (WT) non-transgenic mouse (bottom panels). The levels of intensity cannot be compared between sections which have been subjected to different exposures. (**C**) Densitometry was performed on the mRNA *in situ* hybridization autoradiographs to obtain a profile of regional transgene mRNA distribution. Absolute optical densities were measured in the striatum (striat), inner cortex (deepctx), outer cortex (supctx), entorhinal cortex (entctx), thalamus (thalam), hippocampus CA1 (hipca1), CA3 (hipca3) and dentate gyrus (hpsdg) regions and the molecular (cermol) and granule (cergrn) layers of the cerebellum. Results from lines NES144 line 39, NLS144 line 46 and mutNLS144 line 16 are shown. Correlation coefficients between brain regions from all the lines analyzed (NES144 lines 39, 61 and 68, NLS144 lines 25, 46 and 52, mutNLS144 line 16, NLS20 line 50 and R6/2) revealed that there were no gross differences in the pattern of regional mRNA expression between any two lines. (**D**) Western blot analysis of nuclear and cytoplasmic fractions from whole brains of 2-month-old mice from NLS144 lines 25, 46 and 52, NES144 lines 39 and 61, mutNLS144 line 16 and WT control immunoprobed with a htt specific antibody (S830) are displayed. Open arrowheads point to non-specific background bands in cytoplasmic fractions. (**E**) Analysis of the stacking gel suggests a progressive nuclear aggregate pathology in NLS144 line 46 at 2 and 4 months of age. For purposes of comparison, a sample from NLS144 line 52 is shown at 2 months of age. (**F**) The increase in aggregate pathology in NES144 line 61 in both nuclear and cytoplasmic fractions is shown at 2, 4 and 6 months. (N.B. it is not possible to compare the intensity of the bands in E and F as the blots have been subject to different exposures and therefore such a comparison is not quantitative.) (**G**) Immunoprobing with the htt antibody CAG53b reveals the NLS20 transprotein from line 50 in the cytoplasmic and not in the nuclear fractions (upper arrow, 25 kDa). The lower arrow (17 kDa) indicates the cytoplasmic exon 1 protein from Hdex6 and Hdex27 fractions (6). (D and E) Western blots were reprobed with antibodies to either α-tubulin or Mek1 to check the purity and loading of the cytoplasmic fractions and with histone 2B or HDAC1 to assess the purity and loading of the nuclear fractions. Samples for probing with histone 2B were run on separate 15% gels and thus do not accurately represent the loading of nuclear fractions in the S830 blots. The positions of protein size markers are indicated.

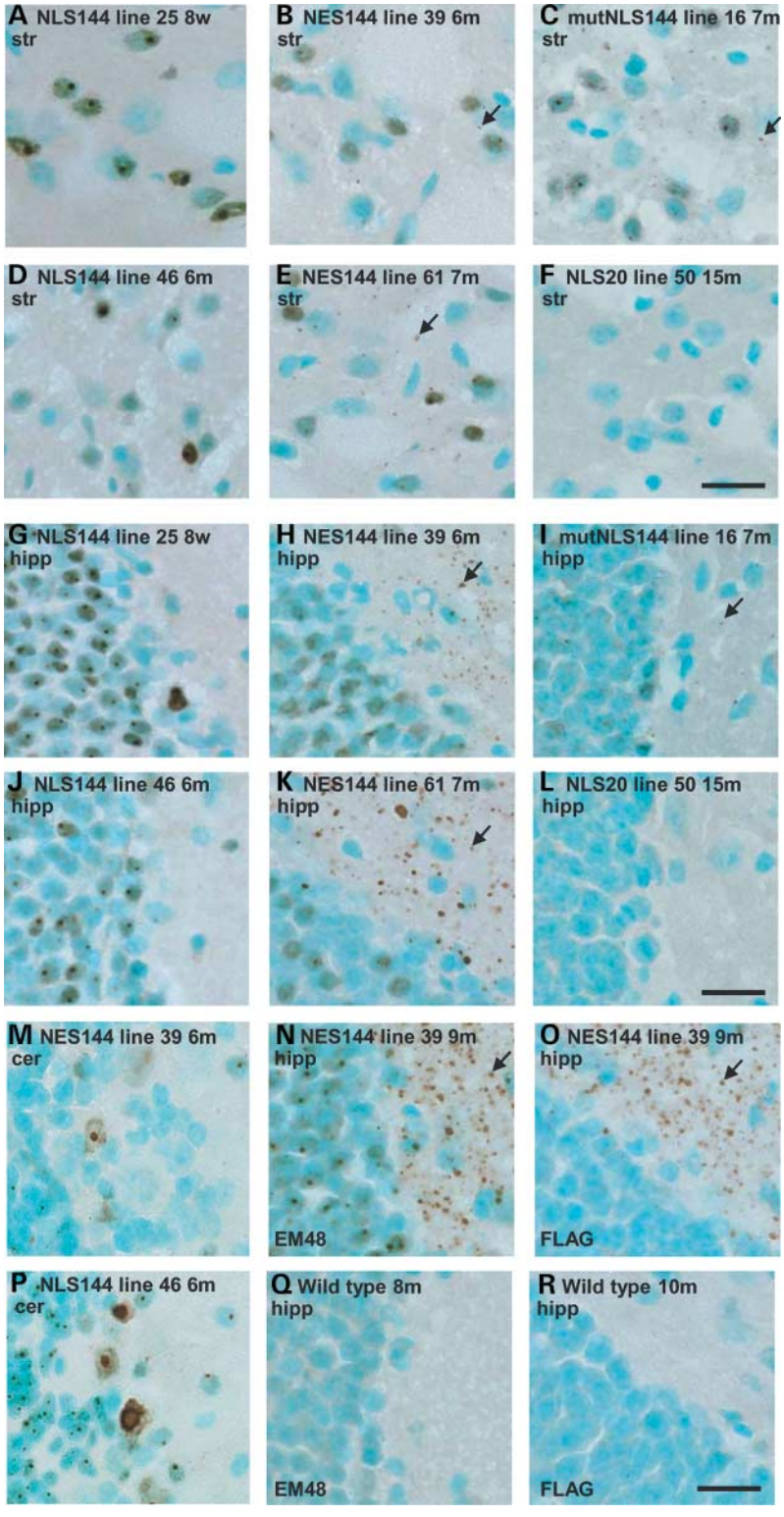

Figure 3. Comparative huntingtin aggregate pathology. Coronal sections from transgenic mouse brains taken at monthly intervals were immunostained with EM48 and counter stained with Methyl green. (**A**–**F**, **G**–**L** and **M** and **P)** representative striatal, hippocampal and cerebellar regions, respectively, from symptomatic mice. NLS144 lines 25 and 46 show no obvious extranuclear aggregation. Both nuclear and extranuclear aggregates are present in NES144 lines 39 and 61 and in mutNLS144 line16. With the exception of NLS144 line 25 (which does not survive beyond 3 months), sections from the Q144 lines were from mice of comparable ages: 6–7 months. The relative amount of extranuclear aggregation differs between brain regions for the NES144 and mutNLS144 lines. NLS20 line 50 sections have been selected from mice at a later time point (15 months) to better demonstrate the absence of an aggregate pathology in this line. (**N** and **O**) contain hippocampal sections from the same NES144 line 39 mouse at 9 months of age immunostained with either EM48 (N) or anti-FLAG (O) and wild-type controls (**Q** and **R**). str, striatum; hipp, hippocampus; cer, cerebellum. Arrows indicate extranuclear aggregates. Scale bar = 20 μm.

progression of nuclear pathologies was present in the NES144 lines as in the NLS144 lines.

Immunostaining of NES144 sections with a FLAG antibody preferentially detected extranuclear aggregates, with extremely weak nuclear aggregate staining when compared with EM48 or S830 labeling on adjacent sections (Fig. 3N, O, P and Q). This is consistent with a model in which the mutant transprotein is retained in the nucleus because formation of aggregation complexes masks the N-terminus encoding the FLAG tag and localization sequences. It also suggests that nuclear and extranuclear aggregates may have different morphologies.

Targeting polyQ to the nucleus accelerates the onset of behavioral phenotypes

NLS144 lines 25, 46 and 52, NES144 lines 39 and 61 and mutNLS144 line 16 were selected for a detailed analysis to compare the onset, nature, progression and duration of behavioral phenotypes. Transgenic mice were indistinguishable from their wild-type littermates at birth, and developed normally until the onset of a behavioral phenotype, if detected. The RotaRod test is a sensitive and highly quantitative measure of motor impairment and a progressive RotaRod impairment was the earliest phenotype detected for all lines tested. Unfortunately, NLS144 line 25 had an aggressive phenotype, which led to its demise after the fifth generation, so insufficient mice were available for RotaRod analysis from this line. For NLS144 line 46, we compared RotaRod performance for males and females and although females tend to perform better than males, the onset and progression of impairment was equivalent in both sexes (Fig. 4A and B). Significant RotaRod deficits (Fig. 4) were detected at the following ages for each line: NLS144 line 46, 3 months ($P = 0.0236$ in males; $P = 0.0065$ in females); NES144 line 39, 4 months ($P = 0.0024$); NES144 line 61, 7 months ($P = 0.0012$); mutNLS144 line 16, 6 months ($P = 0.0266$). There was no significant RotaRod impairment in NLS144 line 52 up to 12 months of age.

We used a modified SHIRPA protocol to probe the spectrum of phenotypes displayed by each line, documenting the time at which each of these phenotypic indicators was first apparent until 12 months of age or endpoint, whichever occurred earlier. SHIRPA is a semi-quantitative battery of tests comprising a comprehensive set of behavioral, functional and pathological screens (22). Phenotypes identified in the transgenic lines and the times at which they first occurred are listed in Table 2.

A progressive RotaRod impairment was the earliest phenotype detected for all lines tested. For the NES144 or NLS144 sets of lines, phenotype onset, defined by both RotaRod and SHIRPA, reflected transgene expression level (Fig. 2A). NLS144 lines 25, 46 and 52 had decreasing levels of expression and progressively later phenotype onsets. A similar inverse relationship between expression levels and phenotype onsets occurs in NES144 lines 39, 61 and 68. Extending this comparison to include mutNLS144 line 16 places it between NES144 lines 39 and 61 and suggests that the NES sequence failed to modify the phenotype.

Comparison of phenotype onsets and expression levels between the NLS144, mutNLS144 and NES144 sets of lines indicates that a much lower NLS144 transgene expression level is required for the manifestation of a phenotype. For example, the NLS144 line 25 transgene is expressed ~3-fold less than the NES144 line 39 transgene (Fig. 2A) and yet produced a dramatically more aggressive phenotype (Table 2). The spectrum of phenotypes recorded was the same, but in NLS144 line 25, the onset of each was accelerated by several months. Similarly, the RNA expression level of NLS144 line 25 is around two-thirds of that in the mutNLS144 line 16 control, yet the phenotypes in line 16 were detected 5–6 months after they first appeared in line 25.

The NLS144 line 25 transprotein was restricted to the nucleus and these mice developed a severe phenotype that displayed all of the behavioral deficits detected in NES144 and mutNLS144 lines. Therefore, a high concentration of mutant transprotein in the nucleus can produce a phenotype indistinguishable on a gross level from mice, which also have mutant protein in the cytoplasm.

Cytoplasmic degeneration can be caused by mutant polyQ in the nucleus

We have generated and characterized transgenic mice in which the transprotein has been targeted to the nucleus (NLS144 lines 25, 46 and 52) together with well-matched lines where it is present in both nuclear and extranuclear locations (NES144 lines 39, 61, 68 and mutNLS144 line 16). We conducted an ultrastructural analysis on brains from NLS144 line 46 and NES144 line 61. EM48 immunogold labeling confirmed the presence of nuclear aggregates in the cerebral cortex and striatum of NLS144 line 46 and NES144 line 61 mouse brains (Fig. 5A and B). In addition, the NES144 line 61 transprotein formed cytoplasmic aggregates primarily found in axons and their terminals (Fig. 5C), with occasional dendritic aggregates (data not shown). There were no obvious cytoplasmic aggregates in NLS144 line 46 mice at the age of 12 months. Therefore, EM analysis confirmed that addition of an NLS results in a nuclear accumulation of mutant htt, whereas the NES was not able to export aggregated mutant htt from the nucleus.

R6/2 mice, which have an earlier onset and faster disease progression than NLS144 line 46 or NES144 line 61, exhibit non-apoptotic dark degenerating neurons in the brain (23,24). We observed very few dark neurons in NLS144 line 46 and NES144 line 61 brains, possibly due to the modest rate of phenotype progression in these lines. We were also unable to detect typical apoptotic neurons in NLS144 line 46 and NES144 line 61 mice, in accordance with R6/2 neuropathology. However, obvious cytoplasmic neurodegeneration was evident in the striatum and cortex in both NLS144 line 46 and NES144 line 61 at 12 and 16 months of age. These pathological changes primarily existed as clustered dark and degenerating organelles adjacent to the intact nucleus, in which no nuclear DNA fragmentation or chromosomal condensation was seen (Fig. 5H). Therefore, cytoplasmic organelle degeneration can occur in the absence

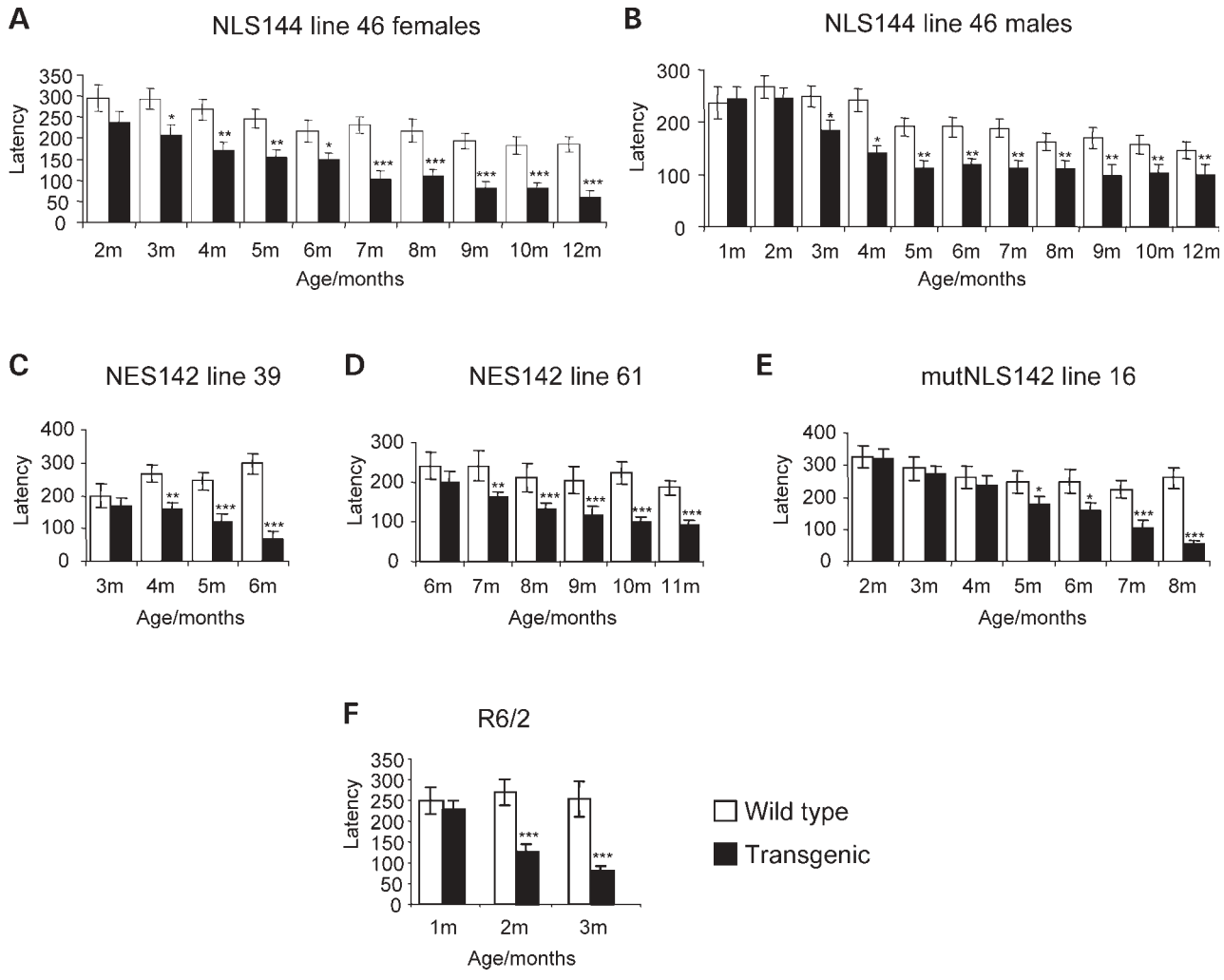

Figure 4. Onset and progression of RotaRod impairment. Mice were tested at monthly intervals. Each bar represents the average latency to fall for either the transgenic (filled bars) or the sex- and age-matched wild-type controls (shaded bars) over the last eight trials for a given time point. (A and B) NLS144 line 46: the RotaRod test was performed on both males and females: (**A**) transgenic females $n = 12$, wild-type females $n = 12$; (**B**) transgenic males $n = 12$, wild-type males $n = 12$. No significant difference in the onset and progression of RotaRod impairment could be detected between the two sexes. (**C**) NES144 line 39: transgenic females $n = 12$, wild-type females $n = 10$. (**D**) NES144 line 61: transgenic males $n = 13$, wild-type males $n = 12$. (**E**) mutNLS144 line 16: transgenic females $n = 10$, wild-type females $n = 10$. (**F**) RotaRod performance of R6/2 mice has been included for comparison: transgenic females $n = 13$; wild-type females $n = 12$. Error bars represent SEM values. $^{*}P \leq 0.05$, $^{**}P \leq 0.01$, $^{***}P \leq 0.001$.

of nuclear degeneration. The dark cytoplasmic bodies are similar in shape and size to lysosomes and mitochondria, suggesting that they are derived from the degeneration of these organelles. This is further inferred by the association of dark cytoplasmic bodies with large vacuoles (Fig. 5E), which may be autophagic vacuoles derived from secondary lysosomes. In NES144 line 61, some degenerated organelles localized with htt aggregates in the same ultrathin section (Fig. 5E and G). However, swollen axons or enlarged axons with reduced electron density or axonal contents as well as disrupted morphology were also found in NLS144 line 46 animals at 12 months (Fig. 5I), indicating that nuclear mutant htt alone can cause cytoplasmic degeneration.

Neither htt aggregate pathology nor cytoplasmic organelle degeneration was observed in NLS20 line 50 mice at the age of 14 months (data not shown).

Extranuclear polyQ does not influence transcriptional dysregulation

Affymetrix GeneChip arrays have been used to generate expression profiles from a wide range of polyQ disease models (25) and extensive data sets have been generated from different brain regions and tissues from the R6/2 mouse model (25–27). Accumulating evidence indicates that transcriptional dysregulation is a central and early pathogenic mechanism in HD, with several possible underlying molecular mechanisms (reviewed in 25). It is not known whether extranuclear polyQ might influence these transcriptional changes. For example, the presence of mutant htt causes the repressor element-1 transcription factor/neuron restrictive silencing factor complex to accumulate in the nucleus and down regulate specific neuronal genes, e.g. BDNF (28). If this is

Table 2. Phenotype profiles of the transgenic lines

Phenotype	NLS144 line 25	NLS144 line 46	NES144 line 39	NES144 line 61	mutNLS144 line 16	R6/2
Rotarod	Not tested	3 m	4 m	7 m	6 m	1.5 m
Tremor	1.5 m	—	5 m	10 m	8 m	3 m
Reduced aggression	2 m	—	5 m	9 m	7 m	3 m
Touch escape	2 m	—	5 m	—	—	3 m
Gait abnormality	2 m	—	6 m	9 m	7 m	3 m
Limb clasping	2 m	—	6 m	9 m	8 m	3 m
Failure at wire maneuver	2 m	—	6 m	11 m	—	3 m
Failure at negative geotaxis	2 m	—	8 m	—	—	3 m
Staring coat	—	—	8 m	12 m	—	3 m
Loss of body tone	2.5 m	—	8 m	12 m	9 m	3 m
Weight loss	2.5 m	—	8 m	12 m	—	2 m (m) 3 m (f)
Hunchback	3 m	—	8 m	12 m	9 m	3 m
Endpoint	3 m	>20 m	10 m	18 m	12 m	3.5 m

Mice were assessed monthly using the primary screen of the SHIRPA protocol until 12 months of age. The age indicates the earliest age at which a phenotype could be detected. The R6/2 mice are included for comparison (m, male; f, female) Endpoint indicates the age at which mice were culled (according to Home Office Project license requirements). — no phenotype detected.

caused by extranuclear interactions with mutant htt, then these decreases in expression might not occur if the mutant transprotein is targeted to the nucleus. To test this, we performed microarray analyses to identify gene expression changes that are present in the NES144 lines and R6/2, but not in the NLS144 lines. Cerebellum was chosen for its profiling, because it is affected in juvenile HD, precision of dissection and known gene expression profiles from previous studies with R6/2 and other HD models (26,27).

Gene expression profiles were generated from NLS144 lines 25 (12 weeks) and 46 (3.5 and 10 months), and NES144 lines 39 (4 and 10 months) and 61 (8 months). Raw data and analysis are available online at http://hdbase.org/cgi-bin/welcome.cgi and at the GEO repository (geo@ncbi.nlm.nih.gov) accession numbers GSE3248. We did not directly compare the NLS144 and NES144 lines but instead concentrated on genes differentially expressed in the transgenic animals relative to their wild-type littermates. The earlier time points: NLS144 line 46, 3.5 months; NES144 line 39, 4 months and NES144 line 61, 8 months broadly correlate to the onset of RotaRod impairment. Expression profiles from cerebella taken at these times showed few expression changes. This is consistent with data from R6/2 mice for which gene expression changes cannot be reliably detected prior to 6 weeks (26), which corresponds to when RotaRod impairment is first apparent. General trends arising from the expression profiles of cerebella from NLS144 line 25, 12 weeks; NLS144 line 46, 10 months and NES144 line 39, 10 months were consistent with the results from previous microarray experiments and were essentially identical to R6/2 profiles and to one another.

Although the general trend was essentially that gene expression changes in the NLS144 and NES144 lines with respect to wild-type were identical, there remained the possibility that some genes could be differentially expressed in the two groups. We therefore compared 10 months cerebella profiles from NLS144 line 46 and NES144 line 39. Genes of interest were defined as those showing consistent differential expression in one line while not changing or changing in the opposite manner in the other line at both early and late time points. This produced a final list of nine genes (Fig. 6A) that could potentially differentiate the NLS and NES lines.

The myelin associated genes: myelin proteolipid protein and myelin-associated oligodendrocyte basic protein (MOBP) appeared to be decreased in the NES144 lines 39 and 61 but not in the NLS line 46. We found the absence of an effect on MOBP expression interesting as a statistically significant decrease in the expression of these genes had been previously detected in the cerebella of R6/2, N171-82Q and DRPLA mice (27). We performed western blots to determine whether specific decreases in mRNA levels had translated to deficits in the protein levels. We found a significant decrease in MOBP cerebellar protein levels in R6/2 (14 weeks) and NES144 line 39 (8 months) but not in NLS144 line 46 at 8 or 17 months of age (Fig. 6B). Therefore, the decrease in MOBP levels corresponds to the mRNA deficits identified by microarray. MOBP protein levels were also marginally decreased (>5%) in the NLS144 line 25 when compared with that in the wild-type. However, this change most likely only reached significance because the error bars were so tight and analysis of a larger sample would be required to confirm whether there is any change in MOBP levels in NLS144 line 25. Further analysis is also required to determine whether the decrease in MOBP in the NES144 and R6/2 lines would be sufficient to contribute to pathogenesis.

DISCUSSION

To further unravel the importance of the subcellular location of the expanded polyQ in HD, we generated 30 transgenic founders expressing exon 1 htt with 20 or 144Q fused to a FLAG tag and either an NLS or an NES. Transgenic mouse lines were established from these founders, and lines were selected for analysis on the basis of transgene mRNA expression levels.

Localization signals did not always result in the intended nuclear or cytoplasmic localization

We were unable to establish a line in which non-pathogenic exon 1 htt was restricted to the nucleus. The NLS20 transprotein was only detected in cytoplasmic fractions on

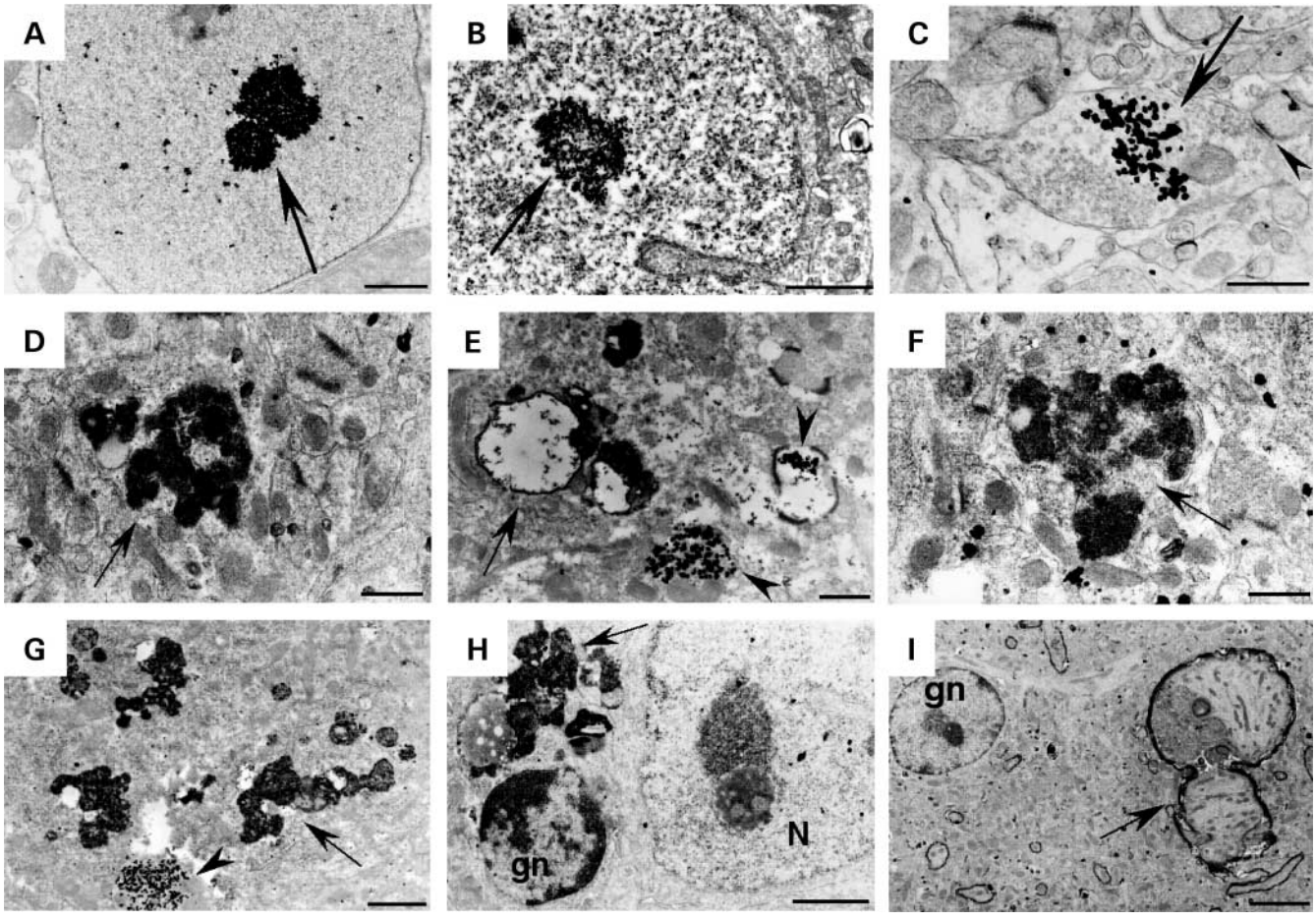

Figure 5. Ultrastructural analysis of NLS144 line 46 and NES144 line 61 brains. Intranuclear aggregates (arrow) labeled by EM48 immunogold are present in the cortex of an NLS144 line 46 mouse at 6 months of age (**A**) and NES144 line 61 mouse at 12 months of age (**B**). Htt aggregates (arrow) are also found in axonal terminals of NES144 line 61 mouse at 16 months of age (**C**). Arrowhead indicates synaptic junction. Scale bars: (A and B) 1 μM, (C) 0.5 μM. Neurodegeneration could also be detected in both NLS144 line 46 and NES144 line 61 mouse brains at 12 and 16 months, respectively (**D**–**G**). Cytoplasmic dark and degenerated bodies (arrows) are present in the cortex (D and E) and the striatum (F and G) of NLS144 line 46 (D and F) and NES144 line 61 (E and G) mice. Arrowheads indicate htt aggregates. (**H**) Degenerated cytoplasmic organelles (arrow) are found near the intact nucleus (N) in NLS144 line 46 mouse striatum. A glial (gn) cell is also seen. (**I**) Micrograph showing a swollen and enlarged axon (arrow) and a normal glial cell (gn) in NLS144 line 46 mouse cortex. Scale bars: 1 μm.

western blots. A potential mechanism for this comes from our recent demonstration that exon 1 htt is exported from the nucleus through its interaction with the nuclear pore protein, Tpr, which overrides the effect of a functional NLS sequence (29). The Tpr binding sequence is located within the first 17 amino acids of exon 1. We hypothesize that the NLS directs the non-pathogenic exon 1 protein to the nucleus only for it to be expelled through interactions with the Tpr protein.

In the case of transgenic proteins with expanded repeats, both NES144 and NLS144 were observed in the nucleus. The NLS most likely successfully directs and concentrates the NLS144 protein in the nucleus. A proportion of the NES144 or mutNLS144 proteins might enter the nucleus by passive diffusion or through interactions with other proteins. We propose that the 144Q exon 1 proteins are then retained in the nucleus because the initiation of the misfolding and aggregation processes masks the Tpr binding sequence (and the NES if applicable), thus preventing the nuclear export of the 144Q protein. Although the Tpr and NES sequences could also become inaccessible through interactions with other proteins, our inability to detect a soluble transprotein in the nucleus in R6/2 or any of the NLS144, NES144 or mutNLS144 lines suggests that it is more likely due to detergent insoluble self-association. In addition, the FLAG antibody was able to detect extranuclear but not nuclear aggregates, which is supportive of nuclear aggregate structure in which the N-terminus is involved in interactions that render it inaccessible, and also hints at different aggregate morphologies in the two compartments.

Thus, we were unable to generate any lines in which a pathogenic exon 1 protein was restricted to the cytoplasm. However, we were able to compare two well-matched series of mice, one in which the mutant transprotein was restricted to the nucleus and the other in which it was present in both the nucleus and the cytoplasm. This allowed us to assess the effects of an exclusively nuclear transgene localization when compared with appropriate controls.

A

Genbank	Gene	NES144 39 4 months	NES144 39 10 months	NLS144 46 3 months	NLS144 46 10 months
AI503362	BTB (POZ) domain containing 3 (Btbd3)	-0.7	-0.9	0.1	-0.1
M25944	carbonic anhydrase 2 (Car2)	-0.5	-0.7	0.2	0
AA716963	isopentenyl-diphosphate delta isomerase (Idi1)	-0.5	-0.8	0.1	0.1
AI839662	myelin-associated oligodendrocytic basic protein (Mobp)	-0.5	-0.7	0.3	0.2
U81317	myelin-associated oligodendrocytic basic protein (Mobp)	-0.6	-0.6	0.1	0.2
M16472	proteolipid protein (myelin) (Plp)	-0.6	-0.8	0	0.1
M37335	proteolipid protein (myelin) (Plp)	-0.7	-0.7	-0.1	0.1
Y13637	tumor necrosis factor (ligand) superfamily, member 7	0.6	0.8	-0.1	-0.1
AA815831	Mus musculus 13 days embryo spinal cord cDNA, RIKEN full-length enriched library, clone:G630020J15 product:unclassifiable, full insert sequence.	-0.1	0.2	-0.6	-0.5
X60980	thymidine kinase 1 (Tk1)	0.2	0.6	-0.8	-0.5
AF107781	potassium voltage gated channel, Shal-related family, member 3 (Kcnd3)	-0.5	-0.1	0.6	7

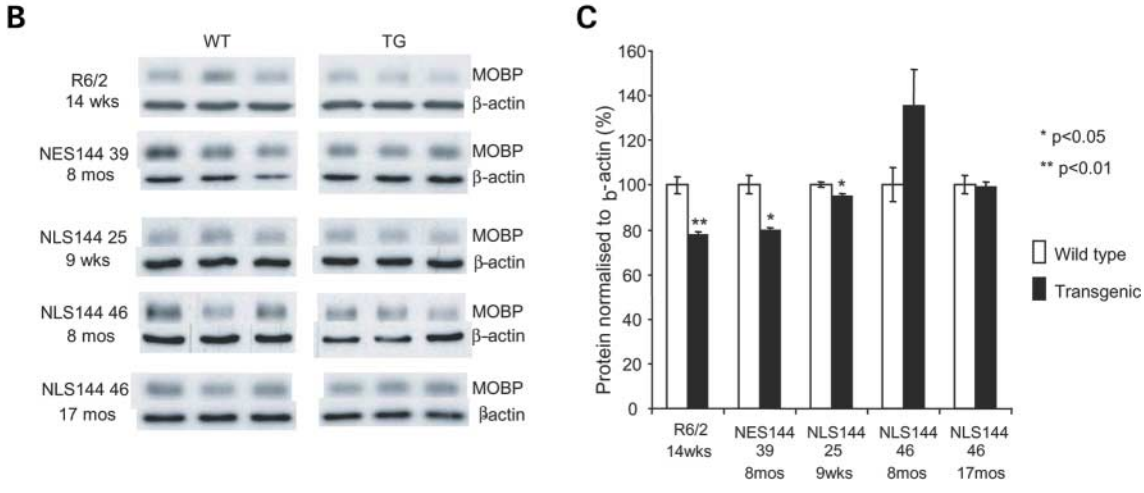

Figure 6. Comparison of NES144 and NLS144 gene expression profiles. (**A**) Cerebellar gene expression profiles from the NES144, NLS144 and R6/2 lines were essentially identical except for the very small number of genes highlighted here. mRNAs altered in NES144 line 39 when compared with littermate controls are shown on the left and those changed in NLS line 46 compared with littermate controls are on the right. Boxes highlighted in pink represent mRNA species that are increased, and boxes highlighted in blue denote decreased mRNA expression levels in the transgenic cerebella when compared with that in the controls. Numbers represent the mean log signal change ($n = 3$ or 4 mice). (**B**) Representative western blots of MOBP protein levels in cerebellar extracts from the transgenic lines as indicated ($n = 3$ shown per genotype). (**C**) Comparative MOBP levels as determined by densitometry of western blots, normalized to β-actin and presented as a percentage of wild-type. MOBP levels were significantly decreased in NLS144 line 25, NES144 line 39 and R6/2 but not in NLS144 line 46. Error bars are SEM, $n = 3$.

Directing mutant exon 1 htt to the nucleus accelerates the onset of a neurological phenotype

Our data clearly demonstrate that targeting N-terminal mutant htt to the nucleus accelerates the onset of the phenotype. The RNA expression level of NLS144 line 25 is around two-thirds of that in the mutNLS144 line 16, yet the phenotypes in line 16 were detected 5–6 months after they first appeared in line 25. This contradicts a recent publication describing transgenic mice in which the N-terminal 171 amino acids of mutant htt with 82Q was directed to the nucleus by the addition of an NLS (18). These mice were reported to develop the same phenotype as the original N17182Q mice but with a delayed phenotype onset. The reason for this discrepancy is most likely because the authors did not generate control lines containing mutant versions of the additional targeting sequence, and the original N17182Q mice do not provide good controls. For example, the transprotein in mutNLS144 line 16 contains exon 1 (as in line R6/2) but with additional FLAG tag and mutant NLS sequences. The RNA expression of the transgene in line 16 is more than 2-fold that in R6/2, but the onset of RotaRod impairment is at 6 months in line 16 as opposed to 1.5 months in R6/2. The additional residues have no effect on transprotein location but dramatically delay phenotype onset and progression and therefore R6/2 could not be used as the control in these experiments. Lines carrying mutant versions of the localization signals must be used when inferring the effects of targeting sequences on phenotype onset

and progression. Consistent with this, the addition of epitope tags to polyQ sequences in *Drosophila* models has been shown to considerably attenuate disease severity (30).

The NLS144 transprotein in line 25 was restricted to the nucleus and these mice developed a severe phenotype that displayed all of the behavioral deficits detected in the NES144 and mutNLS144 lines. Therefore, a high concentration of mutant transprotein in the nucleus can produce a phenotype that is indistinguishable on a gross level from that in mice that also have mutant protein in the cytoplasm. This is consistent with the NLS-N17182Q mice which had a phenotype that closely resembled the original N17182Q mice suggesting that disruption of nuclear processes might be a predominant mechanism of toxicity (18).

Does cytoplasmic mutant polyQ contribute to the neurological phenotype?

NES144 line 39 had an onset of RotaRod impairment at 4 months of age and developed an overt neurological disorder progressing to an endpoint at 10.5 months. Similarly, although NES144 line 61 had a later onset of RotaRod impairment (7 months) and slower disease progression, it too had displayed many SHIRPA phenotypes by 12 months of age. In contrast, although impairment in RotaRod performance could be detected as early as 3 months of age in NLS144 line 46, these mice had not developed any obvious neurological symptoms by 12 months and endpoint had not been reached by 20 months.

An ultrastructural analysis of the cerebral cortex and striatum from NES144 line 61 and NLS144 line 46 brains from mice aged 1 year showed comparable cytoplasmic degeneration manifesting as dystrophic neurites, axonal swelling and organelle degeneration. This surprising finding indicated that nuclear mutant htt alone can cause cytoplasmic degeneration. However, the difference in phenotype presentation between the NES144 lines 39 and 61 and the NLS144 line 46 indicates that this cytoplasmic degeneration is not responsible for the neurological phenotypes detected by SHIRPA.

We found that microarray expression profiles of cerebellar mRNA from NES144 lines 39 and 61 and NLS line 46 when compared to wild-type controls were essentially identical to each other and to previously published profiles of R6/2 mice (26,27). This was even the case for expression profiles from NES144 line 39 and NLS144 line 46 at 10 months of age, a time at which line 39 is close to endpoint and line 46 does not display any overt phenotypes (Table 2). As the mechanisms by which mutant htt is proposed to cause transcriptional dysregulation are global, e.g. chromatin remodeling, impairment of TBP function (25), we would expect that the expression profiles of other brain regions from these lines would also be very similar to each other. It would seem that nuclear transprotein is sufficient for transcriptional dysregulation, which overall does not account for the overt neurological phenotypes identified by the SHIRPA analysis (Table 2). However, in the cerebellum, there were two genes that were downregulated in NES144 line 39 when compared with NLS line 46, which encode components of CNS myelin and may contribute to the NES144 line 39 and 61 phenotypes, e.g. tremors, and therefore merit further investigation. The decreases in CNS myelin components would be consistent with recent reports of decreased white matter volumes throughout the brain in early stage HD (31,32).

To be able to definitively assign the neurological phenotypes observed in NES144 lines 39 and 61 that were not present in NLS144 line 46 as consequences of cytoplasmic mutant polyQ, it is necessary to compare the levels of the mutant protein in the nucleus. Unfortunately, this is impossible to quantify, as the soluble transprotein is never detected in the nucleus in any of these lines. However, non-quantitative immunohistochemistry consistently showed comparable levels of aggregated protein in the neuronal nuclei in brain sections from these two mouse lines, suggesting that there is no dramatic discrepancy between the levels of nuclear protein.

CONCLUSION

We have shown that targeting an N-terminal mutant htt fragment to the nucleus accelerates the onset and progression of a neurological phenotype in transgenic mice. Directing very high levels of mutant protein to the nucleus, as in NLS144 line 25, causes a severe phenotype that displays all of the neurological phenotypes detected in the NES144 lines. However, comparison of NES144 lines 39 and 61 with NLS144 line 46 shows a dramatic difference in the onset and progression of phenotypes despite the comparable (a) accumulation of aggregated mutant polyQ in the nucleus (b) transcriptional profiles and (c) cytoplasmic degeneration. This suggests that the extranuclear mutant polyQ may be contributing to the neurological phenotype in these lines. Specific mechanisms by which this might be occurring have been identified and include, among others, disruption of the microtubule transport pathways (33,34), the inhibition of synaptic function and glutamate release (35,36), mitochondrial calcium defects (37) and excitotoxicty and defects in calcium signaling (38). This series of transgenic mouse lines will provide an invaluable resource to further unravel the mechanisms through which nuclear and extranuclear exon 1 mutant htt contributes to HD pathogenesis. However, to clearly define the role of extranuclear polyQ, it will be essential to generate lines of mice in which a pathogenic exon 1 protein is restricted to the cytoplasm. Therefore, our data underscore the critical role of the nucleus in the pathogenesis of HD but indicate that extranuclear polyQ might also contribute to this process.

MATERIALS AND METHODS

Transgene construction

Plasmids p4G6E4.0 and pSKE4.0 contain a 4 kb *Eco* RI fragment with 3.6 kb of the HD promoter, exon 1 with 18 and 142 CAG repeats respectively and 0.3 kb of intron 1. The plasmids were linearized with *Xcm* I, dephosphorylated and ligated with the FLAG tag (annealed phosphorylated oligonucleotides 40142 and 40143) (Table 3). This placed a methionine codon before the FLAG tag and mutated the methionine at the beginning of exon 1 to an isoleucine.

The FLAG tag containing plasmids were linearized with *Kpn* I, dephosphorylated and ligated with annealed

Table 3. Oligonucleotide sequences

Oligonucleotide	5′–3′ Sequence
33934	GGCGGCTGAGGAAGCTGAGGA
40031	TGTCCGGGTGAGTATGGCTC
40036	TCCCCTCGTGAGAGGACAAGG
40080	CAGAGCCCCATTCATTGCC
40085	TTCATCAGCTTTTCCAGGGT
40142	GACTACAAAGACGATGACGATAAAGGTACCA-TAGTG
40143	ACTATGGTACCTTTATCGTCATCGTCTTTG-TAGTCC
40155	AGATGGACGGCCGCTCAGGTT
40169	CGCCCTGCAGAAAAAACTGGAGGAGCTG-GAGCTGGACGTCGGTAC
40170	CGACGTCCAGCTCCAGCTCCTC-CAGTTTTTTCTGCAGGGCGGTAC
40171	CGCCGCCCAGAAAAAAGCCGAGGAGGCC-GAGGCCGACGTCGGTAC
40172	CGACGTCGGCCTCGGCCTCCTCGGCTTTTTTCT-GGGCGGCGGTAC
40191	CCCTCCAAAAAAGAAGAGAAAGGTA-GACGTCGGTAC
40192	CGACGTCTACCTTTCTCTTCTTTTTTGGAGGGG-TAC
40193	CCCTCCAAAAACTAAGAGAAAGGTA-GACGTCGGTAC
40194	CGACGTCTACCTTTCTCTTAGTTTTTGGAGGGG-TAC
40298	GCTGCACCGACCGTGAGT
40299	CGCAGGCTGCAGGGTTAC
40300	CAGCTCCCTGTCCCGGCGG
40310	GCTTCTTTGCAGCTCCTTCGT
40311	CCAGCGCAGCGATATCG
40312	CGGTCCACACCCGCCACCAG
TG3	TCTGGGTTGCTGGGTCACTCTGTCTCTGCG-GAGCCGGGGG

phosphorylated oligonucleotides containing the sequence for a functional NLS (40191 and 40192), a mutant NLS (40193 and 40194), a functional NES (40169 and 40170) or a mutant NES (40171 and 40172). Resultant plasmids were sequenced prior to *Sac* I and *Eco* RI digestion to yield a microinjection fragment. Sequencing was performed using an ABI377 automated DNA sequencer using a rhodamine dye terminator ready reaction mix (Perkin Elmer). Sequencing primers were 40031, 40155, 40080, 40085, 33934 and 40036 (Fig. 1A).

Generation and maintenance of transgenic mice and genotyping

The microinjection fragments of 1.6/1.9 kb (with 18/142 CAG repeats) were purified from 1.0% agarose gels with a BIOTRAP™ (Schleicher and Schuell) resuspended in $TE_{0.1}$ (10 mM Tris:HCl pH 7.4; 0.1 mM EDTA pH 8.0) at 1.5 ng/μl, filtered through a 0.2 μm centrifuge column (Millipore) and microinjected into (CBA × C57BL/6)F1 pronuclei. Founders were identified by PCR from tail DNA with primer pair 40080 and 40085 in Promega buffer, 2.5 mM $MgCl_2$, 200 μ MdNTPs, 10 ng/μl primers and 0.5 U/μl *Taq* polymerase (Promega). Cycling conditions were 90 min at 94°C, 35 × (30 min at 94°C, 30 min at 60°C, 90 min at 72°C), 10 s at 72°C. This amplified both murine (121 bp) and transgenic htt (194 bp for NES lines,185 bp for NLS lines). Transgenic status of the founders and the first two generations of established lines was confirmed by Southern blot as described (6).

Founders and transgenic progeny were backcrossed to (CBA × C57BL/6)F1 mice (Harlan Olac) with transgenic males bred preferentially. All husbandry procedures (39) were carried out in accordance with Home Office Guidelines. Genotyping was as described earlier and CAG repeat size was determined as previously published (40). Mice were culled by cervical dislocation and tissues were removed for analysis. Either the whole brain was snap-frozen in isopentane or the dissected brain and body regions were snap-frozen in liquid nitrogen prior to storage at −80°C.

RNA extraction and expression analysis

RNA preparation, northern blots and RT–PCR were performed as previously described (6) except that primers 40080 and 40085 were used for RT–PCR. RNA for RQ-PCR was prepared from 30 mg cerebral cortex from animals at 2 months of age using the RNeasy kit (Qiagen). Reverse transcription of 1 μg of total RNA was performed as previously described (6) except the reverse transcriptase was from Invitrogen. The RT reaction was diluted 2.5-fold in nuclease free water (Sigma) and 5 μl was used in a 25 μl reaction containing Taqman master mix (ABI), 300 nM primers and 200 nM probe using the ABI7700 Taqman. Primer sequences for amplification of the htt transgene were 40298 and 40299 and the probe was 40300; and for β-actin, the primers were 40310 and 40311 and the probe was 40312 (Table 3). Estimation of mRNA copy number was determined in triplicate for each RNA sample through comparison to standard curves.

In situ hybridization analysis of transgene expression was performed as previously described (41) with [^{35}S]end-labeled TG3 oligonucleotide probe targeted against a human-specific intron of the human HD transgene sequence (Table 3). Slides were exposed multiple times to Amersham β-max autoradiography film for 2, 7 and 14 days. *In situ* hybridization signal was analyzed by measuring film densities using a computer-based image analysis system (MI, Imaging Research) for striatum, superficial layers of frontal cortex, deep layers of frontal cortex, entorhinal cortex, dentate gyrus, CA1 and CA3 regions of hippocampus, thalamus, granule and molecular cell layers of the cerebellum. Average signal values (absolute optical density) were obtained for each region and correlation coefficients for all brain regions across all of the lines were calculated.

Protein extraction and western blotting

Cerebellar lysates were homogenized in sodium phosphate buffer [20 mM $NaPO_4$ pH 7.4; 1% sodium dodecyl sulfate (SDS)] with 'complete' protease inhibitors (GibcoBRL). Nuclear and cytoplasmic fractions were prepared from snap-frozen whole brain as described (42) except the homogenate was not filtered through cheesecloth, before aliquoting and storing at −80°C.

Tissue lysates (10 μg) or freshly thawed nuclear (40–50 μg) and cytoplasmic fractions (90–100 μg) were

quantified with the BCA protein assay kit (Perbio) and loaded onto 10 and 15% SDS–PAGE gels, blotted onto Hybond-P membranes (Amersham), immunoprobed and detected as described (43). Primary antibodies and dilutions were S830 (1:750), pAb (43); Mek1 (1:3000), pAb (Santa Cruz Biotech); Histone 2b (1:400), pAb (Chemicon); α-tubulin (1:500), mAb (Sigma); β-actin (1:5000), mAb (Abcam Ltd); CAG53b (1:5000), pAb (44); α-HDAC1 (1:10 000), pAb (gift from C. Seiser) and MOBP (1:1000), pAb (Santa Cruz Biotech). HRP-conjugated secondary antibody dilutions were anti-rabbit (1:3000) (Dako); anti-sheep (1:3000) (Chemicon) and anti-mouse (1:5000) (Vectastain).

Film densities of bands were analyzed using a computer-based image-analysis system (MI, Imaging Research).

Phenotype analysis

A Ugo Basile 7650 Accelerating RotaRod for Mice (Linton Instruments) was used to test motor performance in a minimum of 10 transgenic mice and their littermate controls (age and sex-matched) as previously described (39) except acceleration increased from 8 to 80 r.p.m. over a period of 570 s. We performed four trials per day for three consecutive days (12 trials) on a monthly basis, with the first assessment for each group of mice incorporating four trials per day for four consecutive days (16 trials). The averages of the last eight trials per genotype per time point was analyzed using the two-tailed Student's *t*-test. *P*-values of 0.05 or less were taken as being statistically significant.

The SHIRPA screen is a battery of tests (22) of which we assayed: body weight, body position in viewing jar, spontaneous activity, respiration rate, tremor, transfer arousal, locomotor activity, piloerection, startle response, gait, pelvic and tail elevation, touch escape response, positional passivity, visual placing, grip strength, body tone, wire maneuver, trunk curling and limb grasping on tail suspension, skin color, salivation, provoked biting, contact righting reflex, negative geotaxis, fear, aggression, irritability, vocalization, body length, body temperature, urination, defecation, hunched back, stereotypical grooming and any other bizarre behavior. SHIRPA was performed on five transgenic and five wild-type mice for each line studied at monthly intervals. The equipment and protocols necessary to conduct a SHIRPA screen are detailed at http://www.mgu.har.mrc.ac.uk/facilities/mutagenesis/mutabase/shirpa_summary.html.

Immunohistochemistry

Performed on 15 μm coronal sections from isopentane frozen brains using the avidin–biotin system with 3,3′-diaminobenzidine as a chromogen and antibody dilutions were as previously described (45) except for FLAGBioM2 (1:1000), mAb (Sigma).

Ultrastructural analysis and electron microscopic immunohistochemistry

Tissue perfusion, immunogold labeling with EM48 and electron microscopy were as previously described (13).

Microarray analyses

Total RNA was isolated from frozen cerebella by Trizol reagent (Invitrogen) from three to four mice. Residual salts and solvents were removed by RNeasy columns (Qiagen). cRNA synthesis and hybridization to Affymetrix U74Av2 GeneChip sets (Affymetrix, Santa Clara, CA, USA) were performed according to protocols in the Affymetrix Expression Analysis Technical Manual http://www.affymetrix.com/support/technical/manuals.affx. Array images were analyzed and compared using Affymetrix Microarray Suite 5.0 software. Differential expression in the NES and NLS was defined by three criteria. First, probesets had to be within the top 50% of mean signal strengths. Mean signal strength was determined by averaging the signal for each probeset over all NLS, NES and control arrays. Secondly, the absolute value of the mean log signal change in a transgenic line relative to its controls had to be larger than 0.5 at each age profiled. Thirdly, if the gene decreased according to the second criteria in one transgenic line, the mean log signal change in the contrasting transgenic line had to be greater than −0.1, or if the gene increased in the first line, the mean log signal change in the contrasting line had to be less than 0.1.

ACKNOWLEDGEMENTS

We wish to thank Amarbirpal Mahal for genotyping and repeat sizing mice, Olivera Spasic Boscovic and Zhao-Xue Yu for technical assistance and Jamie Tse for help with figures. This work was supported by grants from the Wellcome Trust (051897; 060360; 066270), Huntington's Disease Society of America Coalition for the Cure Program, Hereditary Disease Foundation, Human Frontiers Science Programme (RG0132), Medical Research Council (G9800001), Glendorn Foundation, National Institutes of Health (AG19206; NS41669; NS38106; NS45242).

Conflict of Interest statement: All authors have no conflict of interest.

REFERENCES

1. Bates, G.P., Harper, P.S. and Jones, A.L. (eds) (2002) *Huntington's Disease*, 3rd edn. Oxford University Press, Oxford.
2. DiFiglia, M., Sapp, E., Chase, K.O., Davies, S.W., Bates, G.P., Vonsattel, J.P. and Aronin, N. (1997) Aggregation of huntingtin in neuronal intranuclear inclusions and dystrophic neurites in brain. *Science*, **277**, 1990–1993.
3. Becher, M.W., Kotzuk, J.A., Sharp, A.H., Davies, S.W., Bates, G.P., Price, D.L. and Ross, C.A. (1998) Intranuclear neuronal inclusions in Huntington's disease and dentatorubral and pallidoluysian atrophy: correlation between the density of inclusions and IT15 CAG triplet repeat length. *Neurobiol. Dis.*, **4**, 387–397.
4. Gutekunst, C.A., Li, S.H., Yi, H., Mulroy, J.S., Kuemmerle, S., Jones, R., Rye, D., Ferrante, R.J., Hersch, S.M. and Li, X.J. (1999) Nuclear and neuropil aggregates in Huntington's disease: relationship to neuropathology. *J. Neurosci.*, **19**, 2522–2534.
5. Bates, G.P. and Benn, C. (2002) The polyglutamine diseases. In Bates, G.P., Harper, P.S. and Jones, A.L. (eds), *Huntington's Disease*, 3rd edn. Oxford University Press, Oxford, pp. 429–472.
6. Mangiarini, L., Sathasivam, K., Seller, M., Cozens, B., Harper, A., Hetherington, C., Lawton, M., Trottier, Y., Lehrach, H., Davies, S.W. *et al.* (1996) Exon 1 of the HD gene with an expanded CAG repeat is sufficient to cause a progressive neurological phenotype in transgenic mice. *Cell*, **87**, 493–506.

7. Carter, R.J., Lione, L.A., Humby, T., Mangiarini, L., Mahal, A., Bates, G.P., Dunnett, S.B. and Morton, A.J. (1999) Characterization of progressive motor deficits in mice transgenic for the human Huntington's disease mutation. *J. Neurosci.*, **19**, 3248–3257.
8. Lione, L.A., Carter, R.J., Hunt, M.J., Bates, G.P., Morton, A.J. and Dunnett, S.B. (1999) Selective discrimination learning impairments in mice expressing the human Huntington's disease mutation. *J. Neurosci.*, **19**, 10428–10437.
9. DiFiglia, M. (2002) Huntingtin fragments that aggregate go their separate ways. *Mol. Cell*, **10**, 224–225.
10. Petersen, A., Gil, J., Maat-Schieman, M.L., Bjorkqvist, M., Tanila, H., Araujo, I.M., Smith, R., Popovic, N., Wierup, N., Norlen, P. *et al.* (2005) Orexin loss in Huntington's disease. *Hum. Mol. Genet.*, **14**, 39–47.
11. Strand, A.D., Aragaki, A.K., Shaw, D., Bird, T., Holton, J., Turner, C., Tapscott, S.J., Tabrizi, S.J., Schapira, A., Kooperberg, C.L. *et al.* (2005) Gene expression in Huntington's disease skeletal muscle: a potential biomarker. *Hum. Mol. Genet.*, **14**, 1863–1876.
12. Davies, S.W., Turmaine, M., Cozens, B.A., DiFiglia, M., Sharp, A.H., Ross, C.A., Scherzinger, E., Wanker, E.E., Mangiarini, L. and Bates, G.P. (1997) Formation of neuronal intranuclear inclusions underlies the neurological dysfunction in mice transgenic for the HD mutation. *Cell*, **90**, 537–548.
13. Li, H., Li, S.H., Cheng, A.L., Mangiarini, L., Bates, G.P. and Li, X.J. (1999) Ultrastructural localization and progressive formation of neuropil aggregates in Huntington's disease transgenic mice. *Hum. Mol. Genet.*, **8**, 1227–1236.
14. Saudou, F., Finkbeiner, S., Devys, D. and Greenberg, M.E. (1998) Huntingtin acts in the nucleus to induce apoptosis but death does not correlate with the formation of intranuclear inclusions. *Cell*, **95**, 55–66.
15. Klement, I.A., Skinner, P.J., Kaytor, M.D., Yi, H., Hersch, S.M., Clark, H.B., Zoghbi, H.Y. and Orr, H.T. (1998) Ataxin-1 nuclear localization and aggregation: role in polyglutamine-induced disease in SCA1 transgenic mice. *Cell*, **95**, 41–53.
16. Katsuno, M., Adachi, H., Kume, A., Li, M., Nakagomi, Y., Niwa, H., Sang, C., Kobayashi, Y., Doyu, M. and Sobue, G. (2002) Testosterone reduction prevents phenotypic expression in a transgenic mouse model of spinal and bulbar muscular atrophy. *Neuron*, **35**, 843–854.
17. Jackson, W.S., Tallaksen-Greene, S.J., Albin, R.L. and Detloff, P.J. (2003) Nucleocytoplasmic transport signals affect the age at onset of abnormalities in knock-in mice expressing polyglutamine within an ectopic protein context. *Hum. Mol. Genet.*, **12**, 1621–1629.
18. Schilling, G., Savonenko, A.V., Klevytska, A., Morton, J.L., Tucker, S.M., Poirier, M., Gale, A., Chan, N., Gonzales, V., Slunt, H.H. *et al.* (2004) Nuclear-targeting of mutant huntingtin fragments produces Huntington's disease-like phenotypes in transgenic mice. *Hum. Mol. Genet.*, **13**, 1599–1610.
19. Kalderon, D., Roberts, B.L., Richardson, W.D. and Smith, A.E. (1984) A short amino acid sequence able to specify nuclear location. *Cell*, **39**, 499–509.
20. Fukuda, M., Gotoh, I., Gotoh, Y. and Nishida, E. (1996) Cytoplasmic localization of mitogen-activated protein kinase kinase directed by its NH2-terminal, leucine-rich short amino acid sequence, which acts as a nuclear export signal. *J. Biol. Chem.*, **271**, 20024–20028.
21. Fukuda, M., Gotoh, I., Adachi, M., Gotoh, Y. and Nishida, E. (1997) A novel regulatory mechanism in the mitogen-activated protein (MAP) kinase cascade. Role of nuclear export signal of MAP kinase kinase. *J. Biol. Chem.*, **272**, 32642–32648.
22. Rogers, D.C., Fisher, E.M., Brown, S.D., Peters, J., Hunter, A.J. and Martin, J.E. (1997) Behavioral and functional analysis of mouse phenotype: SHIRPA, a proposed protocol for comprehensive phenotype assessment. *Mamm. Genome*, **8**, 711–713.
23. Turmaine, M., Raza, A., Mahal, A., Mangiarini, L., Bates, G.P. and Davies, S.W. (2000) Nonapoptotic neurodegeneration in a transgenic mouse model of Huntington's disease. *Proc. Natl Acad. Sci. USA*, **97**, 8093–8097.
24. Yu, Z.X., Li, S.H., Evans, J., Pillarisetti, A., Li, H. and Li, X.J. (2003) Mutant huntingtin causes context-dependent neurodegeneration in mice with Huntington's disease. *J. Neurosci.*, **23**, 2193–2202.
25. Luthi-Carter, R. and Cha, J.-H.J. (2003) Mechanisms of transcriptional dysregulation in Huntington's disease. *Clin. Neurosci. Res.*, **3**, 165–177.
26. Luthi-Carter, R., Hanson, S.A., Strand, A.D., Bergstrom, D.A., Chun, W., Peters, N.L., Woods, A.M., Chan, E.Y., Kooperberg, C., Krainc, D. *et al.* (2002) Dysregulation of gene expression in the R6/2 model of polyglutamine disease: parallel changes in muscle and brain. *Hum. Mol. Genet.*, **11**, 1911–1926.
27. Luthi-Carter, R., Strand, A.D., Hanson, S.A., Kooperberg, C., Schilling, G., La Spada, A.R., Merry, D.E., Young, A.B., Ross, C.A., Borchelt, D.R. *et al.* (2002) Polyglutamine and transcription: gene expression changes shared by DRPLA and Huntington's disease mouse models reveal context-independent effects. *Hum. Mol. Genet.*, **11**, 1927–1937.
28. Zuccato, C., Tartari, M., Crotti, A., Goffredo, D., Valenza, M., Conti, L., Cataudella, T., Leavitt, B.R., Hayden, M.R., Timmusk, T. *et al.* (2003) Huntingtin interacts with REST/NRSF to modulate the transcription of NRSE-controlled neuronal genes. *Nat. Genet.*, **35**, 76–83.
29. Cornett, J., Cao, F., Wang, C.E., Ross, C.A., Bates, G.P., Li, S.H. and Li, X.J. (2005) Polyglutamine expansion of huntingtin impairs its nuclear export. *Nat. Genet.*, **37**, 198–204.
30. Marsh, J.L., Walker, H., Theisen, H., Zhu, Y.Z., Fielder, T., Purcell, J. and Thompson, L.M. (2000) Expanded polyglutamine peptides alone are intrinsically cytotoxic and cause neurodegeneration in *Drosophila*. *Hum. Mol. Genet.*, **9**, 13–25.
31. Rosas, H.D., Koroshetz, W.J., Chen, Y.I., Skeuse, C., Vangel, M., Cudkowicz, M.E., Caplan, K., Marek, K., Seidman, L.J., Makris, N. *et al.* (2003) Evidence for more widespread cerebral pathology in early HD: an MRI-based morphometric analysis. *Neurology*, **60**, 1615–1620.
32. Fennema-Notestine, C., Archibald, S.L., Jacobson, M.W., Corey-Bloom, J., Paulsen, J.S., Peavy, G.M., Gamst, A.C., Hamilton, J.M., Salmon, D.P. and Jernigan, T.L. (2004) *In vivo* evidence of cerebellar atrophy and cerebral white matter loss in Huntington disease. *Neurology*, **63**, 989–995.
33. Szebenyi, G., Morfini, G.A., Babcock, A., Gould, M., Selkoe, K., Stenoien, D.L., Young, M., Faber, P.W., MacDonald, M.E., McPhaul, M.J. *et al.* (2003) Neuropathogenic forms of huntingtin and androgen receptor inhibit fast axonal transport. *Neuron*, **40**, 41–52.
34. Gunawardena, S., Her, L.S., Brusch, R.G., Laymon, R.A., Niesman, I.R., Gordesky-Gold, B., Sintasath, L., Bonini, N.M. and Goldstein, L.S. (2003) Disruption of axonal transport by loss of huntingtin or expression of pathogenic polyQ proteins in *Drosophila*. *Neuron*, **40**, 25–40.
35. Li, H., Li, S.H., Johnston, H., Shelbourne, P.F. and Li, X.J. (2000) Amino-terminal fragments of mutant huntingtin show selective accumulation in striatal neurons and synaptic toxicity. *Nat. Genet.*, **25**, 385–389.
36. Li, H., Wyman, T., Yu, Z.X., Li, S.H. and Li, X.J. (2003) Abnormal association of mutant huntingtin with synaptic vesicles inhibits glutamate release. *Hum. Mol. Genet.*, **12**, 2021–2030.
37. Panov, A.V., Gutekunst, C.A., Leavitt, B.R., Hayden, M.R., Burke, J.R., Strittmatter, W.J. and Greenamyre, J.T. (2002) Early mitochondrial calcium defects in Huntington's disease are a direct effect of polyglutamines. *Nat. Neurosci.*, **5**, 731–736.
38. Bezprozvanny, I. and Hayden, M.R. (2004) Deranged neuronal calcium signaling and Huntington disease. *Biochem. Biophys. Res. Commun.*, **322**, 1310–1317.
39. Hockly, E., Woodman, B., Mahal, A., Lewis, C.M. and Bates, G. (2003) Standardization and statistical approaches to therapeutic trials in the R6/2 mouse. *Brain. Res. Bull.*, **61**, 469–479.
40. Mangiarini, L., Sathasivam, K., Mahal, A., Mott, R., Seller, M. and Bates, G.P. (1997) Instability of highly expanded CAG repeats in mice transgenic for the Huntington's disease mutation. *Nat. Genet.*, **15**, 197–200.
41. Benn, C.L., Farrell, L.A. and Cha, J.H. (2004) Neurotransmitter receptor analysis in transgenic mouse models. *Methods Mol. Biol.*, **277**, 231–260.
42. Hallberg, E. (1994) Preparation of nuclei and nuclear envelopes: identification of an integral membrane protein unique to the nuclear envelope. In Celis, J.E. (ed.), *Cell Biology: a Laboratory Handbook*. Academic Press, San Diego. Vol. 1, pp. 613–627.
43. Sathasivam, K., Woodman, B., Mahal, A., Bertaux, F., Wanker, E.E., Shima, D.T. and Bates, G.P. (2001) Centrosome disorganization in fibroblast cultures derived from R6/2 Huntington's disease (HD) transgenic mice and HD patients. *Hum. Mol. Genet.*, **10**, 2425–2435.
44. Scherzinger, E., Lurz, R., Turmaine, M., Mangiarini, L., Hollenbach, B., Hasenbank, R., Bates, G.P., Davies, S.W., Lehrach, H. and Wanker, E.E. (1997) Huntingtin-encoded polyglutamine expansions form amyloid-like protein aggregates *in vitro* and *in vivo*. *Cell*, **90**, 549–558.
45. Smith, D.L., Portier, R., Woodman, B., Hockly, E., Mahal, A., Klunk, W.E., Li, X.J., Wanker, E., Murray, K.D. and Bates, G.P. (2001) Inhibition of polyglutamine aggregation in R6/2 HD brain slices-complex dose–response profiles. *Neurobiol. Dis.*, **8**, 1017–1026.